Stress Compensation in Hafnia/Silica Optical Coatings by Inclusion of Alumina Layers

Introduction

Optical coatings are a critical technology for the successful construction and operation of high-peak-power laser systems. Optical coatings must provide appropriate spectral and photometric performance while maintaining high laser-damage resistance at the wavelength(s) and pulse duration(s) of interest. Additionally, the surface figure of the coated optics must be maintained to preserve the optical performance of the system. Thin-film stresses resulting from the optical coating process, both compressive and tensile, pose a risk to the performance and longevity of the coated components.

Electron-beam deposition of optical coatings has been the standard process for fabricating multilayer coatings for high-peak-power laser applications. The ability to scale the process to large substrates, flexibility in source materials and coating designs, and relatively low cost encourage the selection of this deposition process. Ultimately, however, the determination to date that such coatings produce the highest laser-damage thresholds has led to the use of electron-beam evaporation as the primary deposition process for large, high-peak-power laser components for systems such as OMEGA, OMEGA EP, the National Ignition Facility, Laser Megajoule, and others.

Multilayer coatings consisting of hafnium dioxide and silicon dioxide have been the standard choice for applications at both 1053 nm and 351 nm for these laser systems.[1–6] These materials provide good spectral and uniformity control while maintaining high laser-damage thresholds. Hafnia/silica multilayers, however, exhibit high tensile stresses, particularly on low-thermal-expansion substrates in low-relative-humidity environments, sufficient to provide significant substrate deformation and potentially cracking of the coated surface.[2,7] Modification of the electron-beam deposition process for hafnia/silica coatings has been explored elsewhere, both through evaporation parameters and energetic assistance.[7–9] In this work, the use of aluminum oxide is explored as a means of adjusting the stress in multilayer reflective coatings.

Aluminum oxide has a high bandgap with a corresponding high laser-damage resistance.[10,11] Its relatively low refractive index makes it unattractive choice, however, for the high-index material in interference coating designs since such a refractive index leads to significantly thicker coatings with far greater numbers of layers. Alumina films deposited by electron-beam evaporation have been shown to exhibit tensile film stresses with a very slow diffusion of water, suggesting a relatively dense film structure without large, columnar pores in the coating.[12] The limited number of available coating materials with sufficiently high laser-damage resistance requires the exploration of all available choices. The diffusion behavior of alumina, coupled with its band gap and laser-damage resistance, suggests that further investigation of alumina performance could be beneficial to modifying the performance of hafnia/silica coatings.

Background

Tensile stresses pose significant challenges for implementation of optical components. First, any film stress leads to a deformation of the optic surface in accordance with the mechanical properties of the film and substrate, as described by Stoney's equation:[13]

$$\sigma = \frac{E_s t_s^2}{6(1-\nu_s) t_f R}, \tag{1}$$

where σ is the film stress, R is the radius of curvature of the surface, E_s is Young's modulus of the substrate, ν_s is Poisson's ratio for the substrate, and t_f and t_s are the thickness of the film and substrate, respectively. This describes the impact of the stress on the radius of curvature of the optic surface, leading to changes in the flatness and corresponding optical performance of the component. While mechanically stiff substrate materials of sufficient thickness t_s will exhibit minimal bending from film stress, tensile stresses remain a problem if they lead to cracking, or crazing, of the coating.[14]

Fracture of a coating's surface results when tensile stresses exceed the fracture toughness of the film. Fracture will initiate at a defect in the coating, whether initiated by a scratch at the edge caused by coating tooling or optic mounting, or at a defect within the film such as shown in Fig. 126.49. Fracture also requires a sufficiently thick film in which the stress can be relieved through fracture at the surface, given the strain at that point. This relationship is given by Hutchinson and Suo:[14]

$$h_c = \frac{\Gamma E_f}{Z\sigma^2}, \tag{2}$$

where h_c is the critical coating thickness, Γ is the fracture resistance of the film, E_f is Young's modulus of the film, Z is a geometrical constant dependent on the fracture type (1.976 for film crazing), and σ is the tensile stress in the film. Compressive stresses will not lead to fracture of the coating surface; instead, excessive compressive stresses may lead to a buckling of the coating, potentially with delamination from the surface. This dependence on the thickness of the film relative to the film stress provides a means for understanding failure mechanisms in the coating.

Given the relationships in Eqs. (1) and (2), it is important to reduce the film stress such that optical performance of the component is preserved while fracture of the coating is avoided. Thicker substrates may aid in maintaining flatter optical surfaces and thinner coatings help to prevent cracking, but both of these approaches result in a cost in substrate size and/or achievable coating performance. To provide optimal performance of the optical coating, the magnitude of the tensile film stress must be kept low or ideally moved to a compressive state. Compressive stress also must be kept low in order to maintain surface flatness of the optical component in accordance with Eq. (1).

Stresses in a multilayer coating are a function of the film thickness of each constituent material in the coating, as well as the stress in each material. Equation (1) may be modified to account for the individual stress in each layer by[15]

$$\sigma_1 t_1 + \sigma_2 t_2 + ... + \sigma_n t_n = \frac{E_s t_s^2}{6(1-\nu_s)R}, \tag{3}$$

where σ_i and t_i are now the stress and thickness of each layer of the coating, respectively. Likewise, the total stress in the multilayer will be given by

$$\sigma_{total} = \frac{\sigma_1 t_1 + \sigma_2 t_2 + ... + \sigma_n t_n}{\sum_i t_i} \tag{4}$$

since the individual stress contributions are simply weighted by the relative layer thicknesses of each. Modification of selected layers provides a means of adjusting the overall stress, with the use of three materials providing the ability to calculate the stress according to

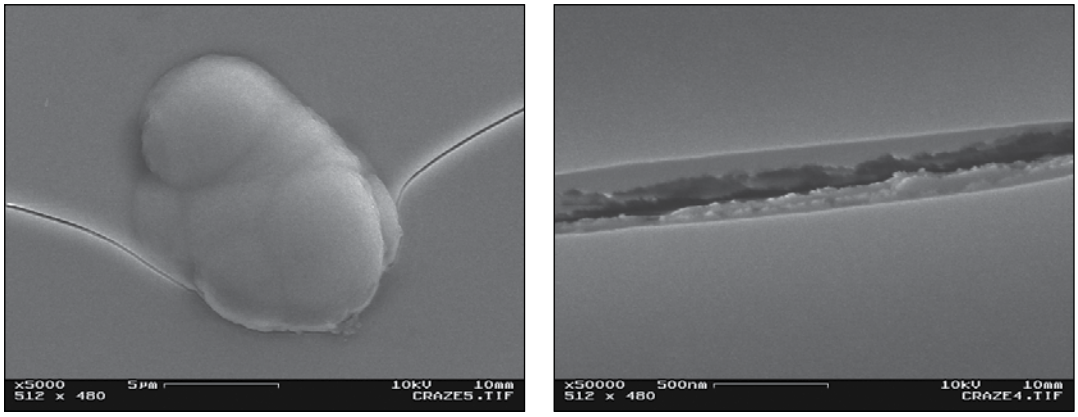

G9047JR

Figure 126.49
Scanning electron microscope imaging of the initiation site and crack that forms as a result of the high tensile stress in the film. A defect site in the coating provides an initiation site for tensile stress failure, while tearing of the film is evident within the crack that forms.

$$\sigma_{\text{total}} = \frac{\sigma_H T_H + \sigma_L T_L + \sigma_A T_A}{T_H + T_L + T_A}, \quad (5)$$

where T_i is now the total thickness of a given material in the entire multilayer since the stress is assumed to be constant for all layers of the same material deposited in the same manner. Subscripts H, L, and A denote hafnia (high refractive index), silica (low refractive index), and alumina, respectively. Given individual material stresses, coating designs may then be modified to yield the desired overall stress.

Experimental Procedure

Coating depositions were performed in a 54-in. coating chamber equipped with quartz heater lamps, dual electron-beam guns, and planetary substrate rotation. Granular silicon dioxide was evaporated from a continuously rotating pan while hafnium metal or aluminum oxide was deposited from a stationary six-pocket electron-beam gun. The baseline coating is a 32-layer hafnia/silica quarter-wave mirror centered at $\lambda_0 = 1053$ nm with a half-wave silica overcoat on fused-silica substrates. Alumina layers were substituted for selected hafnia layers, uniformly distributing the alumina layers throughout the coating. In addition, the first high-index layer on the incident side of the coating was always replaced by alumina to take advantage of its higher band gap in the region of highest electric-field intensity. In this manner, the coating has alumina/silica interfaces but no hafnia/alumina interfaces. The refractive-index profile of such a coating is shown in Fig. 126.50, with the outermost layers on the air side being a half-wave optical thickness of silica, with a quarter-wave optical thickness of alumina immediately beneath it.

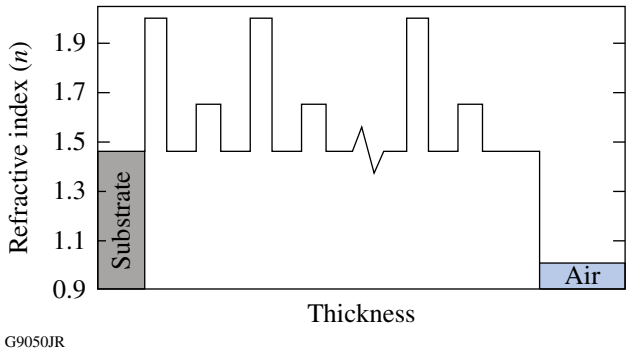

Figure 126.50
Refractive index profile of a hafnia/silica/alumina high-reflector coating. Selected hafnia layers are replaced with alumina layers of equivalent optical thickness with the alumina layers being equally distributed throughout the overall thickness of the coating.

The primary means of altering the coating in this study was through the amount of alumina introduced in the coating design, relative to the overall thickness, as well as through the number of interfaces of each material. Depositions were performed with different overall coating thicknesses, relative numbers of layers and associated interfaces, and individual layer thicknesses. Deposition parameters such as oxygen backfill pressures, deposition rate, and substrate temperature remained constant throughout, in an effort to maintain a consistent film stress for each material between depositions.

Spectral measurements were performed on a Perkin-Elmer Lambda 900 spectrophotometer operating in transmission at normal incidence. The spectrophotometer environment was maintained at 0% relative humidity in order to eliminate optical thickness variations as a result of film water content. Photometric measurements were executed on a laser-based reflectometer system, again in a nitrogen-purged environment to achieve 0% relative humidity; measurements were performed at a constant wavelength while scanning the incident angle on the substrate. The measurement procedure incorporates a dual-beam configuration, using lock-in amplifiers and a chopped signal to minimize signal noise. Extended integration times at each point in the measurement scan further improve the quality of the measured result.

Surface flatness measurements of the 1-in.-diam substrates were performed on a Zygo New View white-light interferometer in a nitrogen-purged enclosure at approximately 0% relative humidity. Samples were purged for 15 h prior to measurement to stabilize the coating stress; measurement routines were automated to ensure consistent purge times. Samples measured after 6 h of purging exhibited irregular measurement results, with a significant decrease in correlation with deposition parameters. Measurements were corrected for cavity irregularity by referencing a $\lambda/50$ calibration flat, and all measurements subtracted the pre-coating flatness measurement of the individual substrate. Samples were supported on a three-point ball bearing mount, with each point positioned 120° apart at 65% of the radius of the substrate to minimize distortion caused by gravity in mounting. The uncoated surface of the samples was measured to avoid interferometric phase errors resulting from the coating. Film stresses based on these surface measurements were compared to those carried out on 310-mm-diam × 14-mm-thick fused-silica substrates measured on an 18-in. Zygo interferometer, with calculated stresses agreeing to within ±8 MPa. Film stresses were also compared to measurements taken in a custom vacuum cell on the Zygo New View; vacuum film stresses were measured to be approximately 8 MPa more tensile than those determined in a

nitrogen environment. Given the relative difficulty in making in-vacuum measurements, this shift in determined film stress was considered acceptable at this time.

Laser-damage testing was performed using 1-ns pulses at a wavelength of 1053 nm. The irradiation spot size, illuminated by a 2-m-focal-length lens, was 600 mm, making it possible to use fluences up to 100 J/cm^2. The sample was inspected under 110× magnification using dark-field microscopy, with an observable change in the surface being defined as damage. Testing may be targeted on defects present in the coating, as a means of identifying the weakest points in the film structure, or on sites that appear pristine, as a means of evaluating the maximum-possible damage threshold for a clean substrate and zero-particulate process. Modes of testing included 1-on-1, where each site on the substrate is illuminated only once, and N-on-1, where the fluence on a given site is gradually ramped through a series of shots until damage is observed.[16]

Results and Discussion

The goal of this work is to alter the tensile stress in the hafnia/silica multilayer coatings, shifting it to a low-magnitude compressive stress to eliminate the risk of cracking the coating while minimizing substrate deformation. Observations of current hafnia/silica coatings in vacuum have indicated that multilayers of greater-than-5-μm total film thickness consistently exhibit tensile stress failures in accordance with Eq. (2), providing the motivation for this effort. In addition, such coatings have tensile stresses of 80 MPa or greater, significantly deforming the substrate surface.[4,9] Since polarizer coatings for use in the near-infrared cannot be realized with coatings of less than 5-μm thickness, the stress in the film must be shifted to a more compressive state.[4]

Evaporated alumina films have been reported in the literature as both tensile and compressive.[11,17] The films being studied were found to have a tensile stress when deposited as a monolayer, with a stress of the order of 70±15 MPa. This would suggest alumina is not a viable material for compensation of tensile stresses in high-damage-threshold coatings since it would not offset the tensile stress generated in high-refractive-index hafnia layers. Composite film stresses in hafnia/silica multilayers, however, were tensile, but alumina/silica multilayers remained quite compressive. This could in part be a result of the magnitude of the tensile stress in alumina being less than that in hafnia, allowing it to be compensated by the compressive silica stress.

The film stresses as measured in the hafnia/silica multilayers, alumina/silica multilayers, and the hafnia/alumina/silica (hybrid) multilayers indicate an unexpected interaction between the different layer materials. The hybrid three-material coating design is more compressive than either of the two-material designs; given the relative proportion of materials in each design, this should not be possible in order for Eq. (5) to be valid for all coatings using comparable stress values for the materials in each. This suggests that a modification to Eq. (5) is necessary, possibly to account for inhomogeneous layer stresses and/or interfacial effects.[18] Either effect will be a function of the number of interfaces of the given material, so Eq. (5) is modified to a form

$$\sigma_{\text{total}} = \frac{\sigma_{\text{H}} T_{\text{H}} + \sigma_{\text{L}} T_{\text{L}} + \sigma_{\text{A}} T_{\text{A}}}{T_{\text{H}} + T_{\text{L}} + T_{\text{A}}} + \sigma_{\text{H/L}} I_{\text{H/L}} + \sigma_{\text{A/L}} I_{\text{A/L}}, \qquad (6)$$

where $\sigma_{\text{H/L}}$ and $\sigma_{\text{A/L}}$ are the stresses resulting from interfacial and film-growth effects at each of the hafnia/silica ($I_{\text{H/L}}$) and alumina/silica ($I_{\text{A/L}}$) interfaces, respectively. The number of interfaces in the coating design is counted for each combination of materials, and since both hafnia and alumina have silica layers above and below each layer, the directional dependence is eliminated.

It is possible to determine values for each of the five stresses included in Eq. (6) by establishing a linear series of five equations for simultaneous solution. The six depositions provide a means of calculating the stresses six times, by eliminating one of the depositions from consideration for each calculation. The calculation is most readily constructed in matrix form, for five given depositions:

$$\begin{pmatrix} T_{\text{H1}} & T_{\text{L1}} & T_{\text{A1}} & I_{\text{H/L1}} & I_{\text{A/L1}} \\ T_{\text{H2}} & T_{\text{L2}} & T_{\text{A2}} & I_{\text{H/L2}} & I_{\text{A/L2}} \\ T_{\text{H3}} & T_{\text{L3}} & T_{\text{A3}} & I_{\text{H/L3}} & I_{\text{A/L3}} \\ T_{\text{H4}} & T_{\text{L4}} & T_{\text{A4}} & I_{\text{H/L4}} & I_{\text{A/L4}} \\ T_{\text{H5}} & T_{\text{L5}} & T_{\text{A5}} & I_{\text{H/L5}} & I_{\text{A/L5}} \end{pmatrix} \times \begin{pmatrix} \sigma_{\text{H}} \\ \sigma_{\text{L}} \\ \sigma_{\text{A}} \\ \sigma_{\text{H/L}} \\ \sigma_{\text{A/L}} \end{pmatrix} = \begin{pmatrix} \sigma_{\text{total1}} \\ \sigma_{\text{total2}} \\ \sigma_{\text{total3}} \\ \sigma_{\text{total4}} \\ \sigma_{\text{total5}} \end{pmatrix}, \qquad (7)$$

where σ_{total_i} are the measured stress values of the multilayer coatings, after having stabilized with age. Rearranging this for solution yields

$$\begin{pmatrix} T_{\text{H1}} & T_{\text{L1}} & T_{\text{A1}} & I_{\text{H/L1}} & I_{\text{A/L1}} \\ T_{\text{H2}} & T_{\text{L2}} & T_{\text{A2}} & I_{\text{H/L2}} & I_{\text{A/L2}} \\ T_{\text{H3}} & T_{\text{L3}} & T_{\text{A3}} & I_{\text{H/L3}} & I_{\text{A/L3}} \\ T_{\text{H4}} & T_{\text{L4}} & T_{\text{A4}} & I_{\text{H/L4}} & I_{\text{A/L4}} \\ T_{\text{H5}} & T_{\text{L5}} & T_{\text{A5}} & I_{\text{H/L5}} & I_{\text{A/L5}} \end{pmatrix}^{-1} \times \begin{pmatrix} \sigma_{\text{total1}} \\ \sigma_{\text{total2}} \\ \sigma_{\text{total3}} \\ \sigma_{\text{total4}} \\ \sigma_{\text{total5}} \end{pmatrix} = \begin{pmatrix} \sigma_{\text{H}} \\ \sigma_{\text{L}} \\ \sigma_{\text{A}} \\ \sigma_{\text{H/L}} \\ \sigma_{\text{A/L}} \end{pmatrix}. \qquad (8)$$

The six possible solutions, based on elimination of each of depositions 1–6, are summarized in Table 126.VIII.

Table 126.VIII. Solutions to the system of equations describing the individual stress contributions. Only solutions B and F fit the constraints of the problem.

	A	B	C	D	E	F
σ_H	–200.5	234.3	–5869.5	–252.3	NaN	246.1
σ_L	283.9	–92.8	4367.0	248.4	NaN	–81.0
σ_A	–1058.0	–622.9	–5024.7	1.2×10^{18}	NaN	–630.9
$\sigma_{H/L}$	–0.8	0.6	–8.9	0.1	NaN	0.1
$\sigma_{A/L}$	3.9	3.9	–0.8	-7.9×10^{15}	NaN	3.9

Analysis of the results shows a number of the mathematical solutions do not fit the parameters of the problem. Based on single-layer stress measurements, σ_H is expected to be of the order of 200 MPa and σ_L is of the order of –80 MPa. Only solutions B and F appear to fit the constraints of the problem. While the solutions are very similar, the calculated stress in the alumina films is excessively compressive; this may be due to inhomogeneous stresses that are poorly described by Eq. (6), errors in the stress measurements, or other effects. Given that the magnitude of the stress in the alumina layers is expected to be a maximum of ±100 MPa, rather than the –600 MPa calculated, the modeled values fit the mathematical constraints of the system of equations without necessarily identifying the physical stress contributions accurately.[11] Using an average solution of B and F for coating designs containing different numbers of alumina layers, the determined stress is compared to measured values for selected coatings in Fig. 126.51. While the various stress contributions may not be appropriately distributed among the film materials, the model does provide an indication of the trends in expected film stress for a composite hafnia/silica/alumina coating.

The previous results were used to predict the stresses likely to be achieved for two additional coating depositions, with designs {(HL)^3 [AL(HL)^3]^3 A2L} designated sample #7 and {[AL(HL)^2]^5 A2L} designated #8, where A, L, and H represent quarter-wave optical thicknesses at 1053 nm of alumina, silica, and hafnia, respectively, coefficients indicate a multiple of quarter-wave thickness, and superscripts signify the repetition of that portion of the coating design. The key difference with these hybrid designs is the alteration of the alumina content and the number of alumina/silica interfaces. Calculation of the expected film stress upon aging, using an average of solutions B and F, yields stresses of –11 MPa for #7 and –49 MPa for #8. Calculated stresses based on the measured surface flatness of samples #7 and #8 resulted in –34.5 MPa and –77 MPa, respectively, in both instances understating the compressive stress in the film. While the inaccuracy in the model's prediction is undesirable, the presence of additional compressive stress avoids the risk of tensile stress failure.

The developed model provided general trends for the stress in the film but yielded errors in the predicted stress of –23.5 MPa and –28 MPa in samples #7 and #8. While efforts have been taken to account for the stresses in each material and any differences in stresses attributed to the number of interfaces, no allowance has been made for the potential modification of the stress in one material resulting from the presence of a different material in the multilayer coating. In particular, alumina has been shown to inhibit diffusion of water; it is likely that the presence of alumina layers influences the hydrolysis of silica, with the aging of the film to a more-tensile state over time being largely avoided.[4,6] Refining the model to include such effects would require that all samples contain similar materials, and that the stress in any given layer be a function of the layers above it. The complexity of the model would increase significantly, in order to provide a functional dependence of the stress in each layer to all layers to the incident side, as well as the relative porosity. It is currently expected that such complexity is necessary, however, to fully describe the influence of alumina on the stresses in a hafnia/silica film.

It is suggested by the observed stresses that the changes in coating stress caused by the inclusion of alumina layers are a result of the reduced diffusion of water through the coating

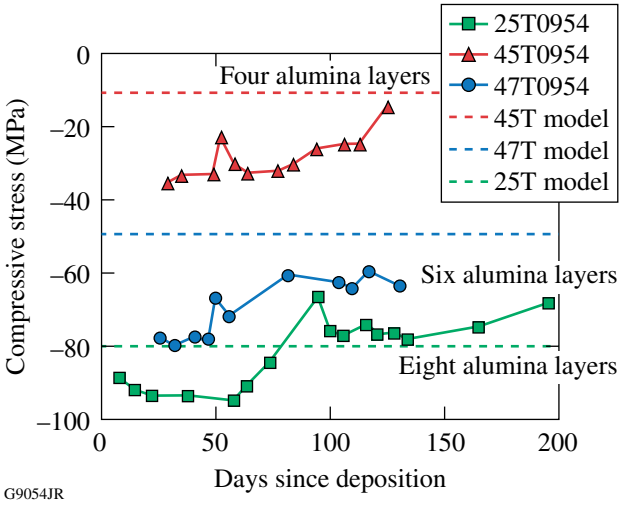

Figure 126.51
Influence of the number of alumina layers on the resulting stress in the multilayer coating. Use of a greater proportion of alumina instead of hafnia shifts the composite multilayer stress more compressively, making the coating suitable for use in a dry or vacuum environment.

structure. As shown in Fig. 126.52, the stress in an alumina/hafnia/silica coating exhibits a very slow drift as the coating is dried in a nitrogen-purged environment. This leads to a strong time dependence for all measured values of stress in order to stabilize the coating performance as much as possible. This uncertainty makes it very difficult to precisely determine the stress of coatings containing alumina since even after a week of drying time, the stress is not fully stabilized.

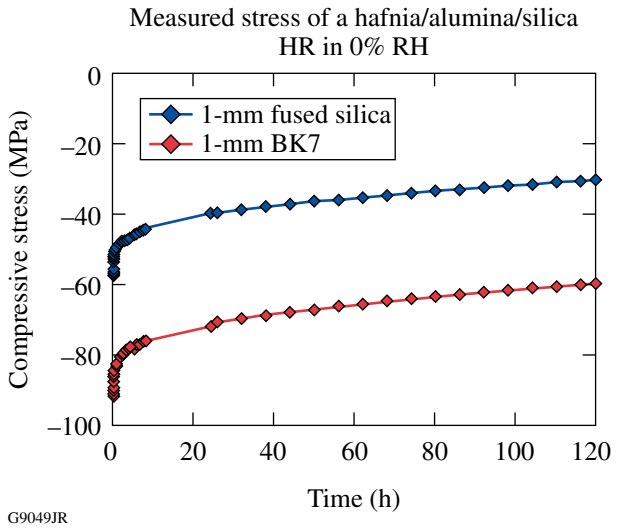

Figure 126.52
Change in stress in an alumina/silica coating as a function of time in dry nitrogen. Note that the stress changes quite slowly, leading to instability in the optical performance over an extended period of time since the surface flatness continues to change.

Implementation

A key advantage of this type of coating modification is that it can be readily performed in a standard evaporation system with minimal equipment changes required. This process was implemented in a 1.8-m coating chamber to alter the stress in a 0.9-m-aperture polarizer coating for use in vacuum on the OMEGA EP Laser System, as previously produced with evaporated hafnia/silica.[4] To integrate this process, the standard six-pocket electron-beam gun used for hafnium metal evaporation was replaced with an EB Sources large-capacity, 12-pocket electron-beam gun, providing additional capacity for alumina evaporation. All deposition monitoring was performed with weighted averaging using an Inficon IC5 and three SensorsTech cartridge-type quartz crystal monitors mounted under stationary uniformity-correction masks, with the substrate mounted in a counter-rotating planetary rotation system.[19,20] Silica was deposited using granular silica in a continuously rotating EB Sources large-capacity, pan-type electron-beam gun.

The original 48-layer polarizer coating design developed for this application was replaced with a 50-layer design containing four alumina layers, with all alumina layers adjoining only silica layers.[4] The alumina layers are nominally one quarter-wave optical thickness, except the layer on the substrate, which is approximately three quarter-waves in optical thickness. The coating design was fully optimized with Optilayer refinement to maximize the photometric coating performance.[21] The alumina layers were inserted every 16th layer, such that the layer on the substrate was alumina and the final high-index layer was alumina. The outermost layer of the coating remained a thick silica layer of greater than one half-wave optical thickness. The overall coating thickness was 9.1 μm, requiring approximately 10 h of deposition time. Cross-sectional scanning electron microscope images of the completed polarizer coating are shown in Fig. 126.53, with the alumina layers appearing very similar to the surrounding silica layers; only the film microstructure differentiates it from the adjoining layers.

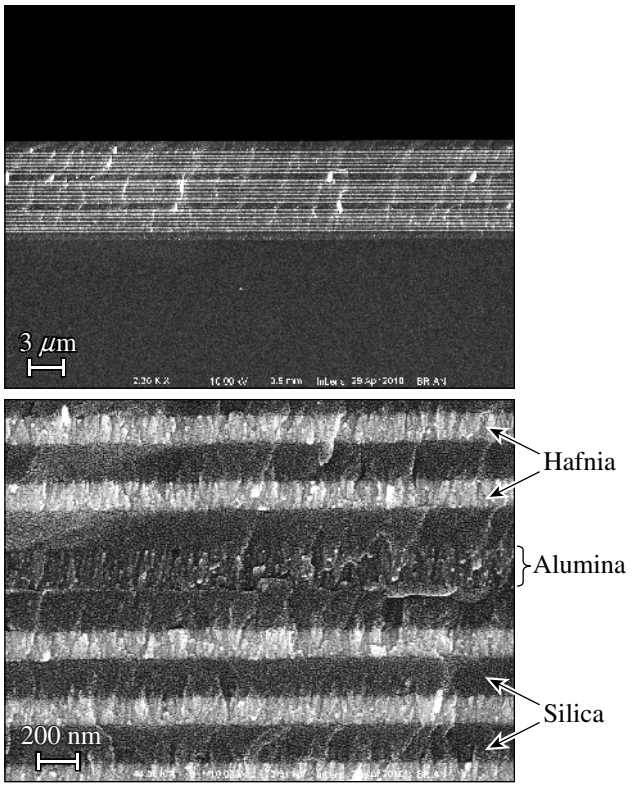

Figure 126.53
Cross-sectional scanning electron micrographs of the polarizer coating modified with four alumina layers. The alumina layers appear to have a more-columnar structure than the surrounding silica layers, which appear amorphous. The hafnia layers appear columnar and much brighter in the image.

Coating performance was measured using a laser-based photometer, providing a highly collimated source, a precise angle of incidence, and high polarization contrast. The performance of this polarizer is shown in Fig. 126.54, indicating *p*-polarized transmission of greater than 98% through the component over an angular range of nearly 9° incidence; polarizer contrast, defined as T_p:T_s, exceeds 200:1 over 8° of this range. In wavelength space, this component has a useful bandwidth of 30 nm after accounting for slight uniformity errors over the 0.9-m aperture and installation alignment tolerances.

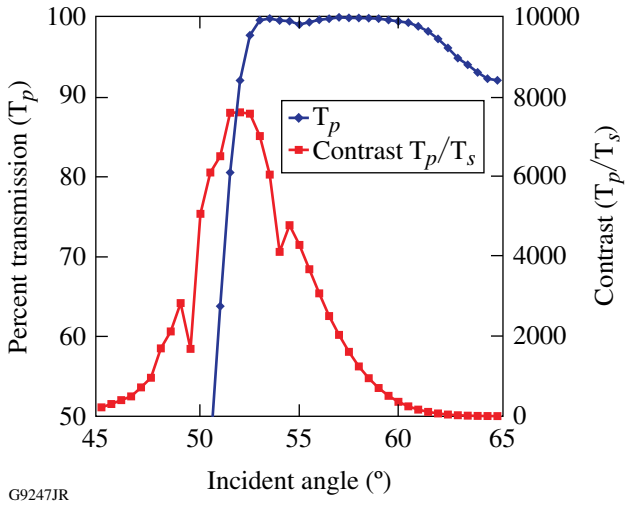

Figure 126.54
Photometric measurement of short-pulse polarizer Z011 installed on OMEGA EP, utilizing alumina for stress control in a dry environment. This polarizer coating provides high transmission and contrast over a wavelength range of 30 nm with incident 1053-nm light.

Laser-damage testing of this coating using a 1053-nm laser with *s*-polarized light in a 1:1 mode indicated damage thresholds of greater than 74 J/cm^2 when tested at 1 ns (clean sites, with no testing performed above this fluence) and 44 J/cm^2 when targeting defects visible using dark-field microscopic inspection.[16] Transmitted laser-damage tests in *p*-polarization remained above 20 J/cm^2. Stress measurements indicate the coating on a BK7 substrate maintains a compressive stress of approximately –100 MPa when measured in an N_2-purged environment at 0% relative humidity. This controlled compressive stress provides a coating that will not fail in tension, even when used in a vacuum environment. As noted previously, the slow drift in film stress as a function of drying time makes it very difficult to accurately determine the stress, with an expected measurement uncertainty of the order of ±20 MPa.

While this coating effort was highly effective—far exceeding the performance requirements for this component—the use of alumina poses significant challenges to the successful implementation in the laser system. The diffusion-barrier properties of the coating significantly restrict the movement of water into and out of the film structure, leading to very slow changes in the coating stress and photometric performance as the relative humidity changes. This change in photometric performance was measured for the polarizer coating, initially stored in an ambient-humidity environment, over a period of multiple days in an N_2-purged, 0%-relative-humidity environment as shown in Fig. 126.55. The coating performance undergoes a substantial change in photometric performance, requiring days or even weeks of recovery time if the optic is stored for long periods in an ambient-humidity environment. Provided the water penetration is slow, short exposure times during installation and alignment can be overcome relatively quickly.

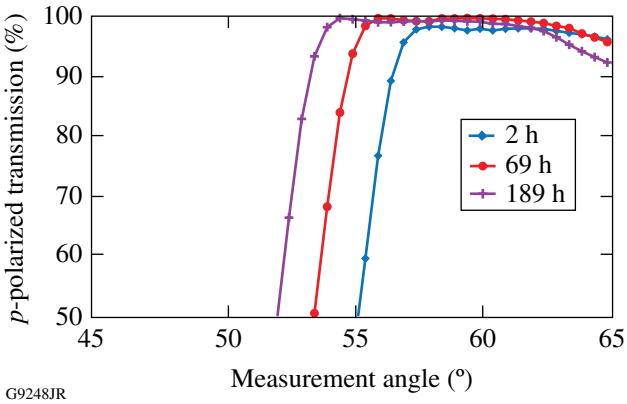

Figure 126.55
Change in photometric performance of a hafnia/silica polarizer coating containing alumina layers. Note that similar to the stress changes in Fig. 126.52, the optical performance of the coating changes significantly over an extended period of time in a dry nitrogen environment. In this case, measurements were performed over a period of approximately 8 days.

The slow drift in performance may be overcome by maintaining the storage and transport of such coatings in a dry atmosphere, while minimizing exposure to humid air during installation and use. Initial evaluation suggests the movement of water into the coating also takes place over a long time scale, as evidenced by the "mottled" appearance that develops as the coating is exposed to moist, ambient air. It is understood that moisture penetration through defect sites in the coating leads to the localized exchange of water for void in the coating, resulting in an increase in the optical thickness and a change

in the color of the coating as shown in Fig. 126.56. Over time, diffusion of the water within the coating structure will bring the water content in the coating to equilibrium, with the coating once again appearing to be a consistent color as the individual moisture-penetration sites through the diffusion barrier coalesce, eliminating the mottled appearance. Alumina is a highly effective diffusion barrier to water penetration and, as such, may require many days of exposure to moist air before the coating once again appears uniform. As shown in Fig. 126.56, a hafnia/silica coating containing alumina barrier layers continues to exhibit a mottled appearance 2 days after deposition. The alumina is quite dense, with isolated defects providing a path for the moisture through the layer, with the surrounding hafnia/silica layers in the multilayer remaining relatively porous.

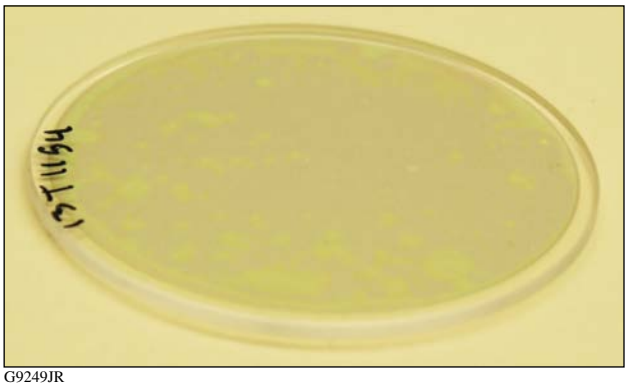
G9249JR

Figure 126.56
Multilayer dielectric coating containing alumina layers 2 days after deposition. Note the "mottled" appearance of the coating color in reflection, indicating an irregular absorption of water into the coating structure.

Conclusions

The inclusion of alumina layers in standard hafnia/silica high-reflectance coatings leads to a significantly more compressive overall film stress, enabling one to use such coatings in vacuum environments on low-thermal-expansion substrates without the risk of tensile-stress failure causing cracking, or crazing, of the film. The use of multiple designs incorporating different numbers of layers, numbers of interfaces, and thicknesses of the constituent materials provides the opportunity to determine the individual contributions of hafnia, silica, and alumina to the overall stress in the multilayer optical coating—a contribution found to be very different than that expected by monolayer stresses. Additionally, interfacial effects were incorporated to account for the inhomogeneous film stresses as each layer was formed. Such calculations, while likely not appropriately allocating the stress contributions of each material, have been demonstrated to provide a somewhat predictive ability for arbitrary multilayer coating designs. The stress in hafnia/silica coating designs, including alumina stress compensation layers, has been demonstrated to agree with theoretical predictions, and hafnia/silica/alumina films can be manufactured without degradation of spectral performance or laser-damage resistance. This process was used to produce large-aperture polarizer coatings for use in an N_2-purged environment on OMEGA EP. It has been shown that such coating designs may be readily implemented using standard electron-beam evaporation systems, are easily scaled to large-aperture substrates, and provide a means of addressing the need for vacuum-use coatings in pulse-compressed laser systems. The slow diffusion of water in such coatings poses some difficulties in implementation, but this may be overcome by storage in a low-relative-humidity environment.

ACKNOWLEDGMENT

The authors wish to express their appreciation to Alex Maltsev for his efforts on the fabrication of extremely high quality, high-aspect-ratio substrates for this study.

This work was supported by the U.S. Department of Energy Office of Inertial Confinement Fusion under Cooperative Agreement No. DE-FC52-08NA28302, the University of Rochester, and the New York State Energy Research and Development Authority. The support of DOE does not constitute an endorsement by DOE of the views expressed in this article.

REFERENCES

1. R. Chow *et al.*, Appl. Opt. **32**, 5567 (1993).
2. J. F. Anzellotti, D. J. Smith, R. J. Sczupak, and Z. R. Chrzan, in *Laser-Induced Damage in Optical Materials: 1996*, edited by H. E. Bennett *et al.* (SPIE, Bellingham, WA, 1997), Vol. 2966, pp. 258–264.
3. J. B. Oliver, J. Howe, A. Rigatti, D. J. Smith, and C. Stolz, in *Optical Interference Coatings*, OSA Technical Digest (Optical Society of America, Washington, DC, 2001), Paper ThD2.
4. J. B. Oliver, A. L. Rigatti, J. D. Howe, J. Keck, J. Szczepanski, A. W. Schmid, S. Papernov, A. Kozlov, and T. Z. Kosc, in *Laser-Induced Damage in Optical Materials: 2005*, edited by G. J. Exarhos *et al.* (SPIE, Bellingham, WA, 2005), Vol. 5991, pp. 394–401.
5. J. B. Oliver, S. Papernov, A. W. Schmid, and J. C. Lambropoulos, in *Laser-Induced Damage in Optical Materials: 2008*, edited by G. J. Exarhos *et al.* (SPIE, Bellingham, WA, 2008), Vol. 7132, p. 71320J.
6. H. Leplan *et al.*, J. Appl. Phys. **78**, 962 (1995).

7. D. J. Smith, M. McCullough, C. Smith, T. Mikami, and T. Jitsuno, in *Laser-Induced Damage in Optical Materials: 2008*, edited by G. J. Exarhos *et al*. (SPIE, Bellingham, WA, 2008), Vol. 7132, p. 71320E.

8. E. Lavastre *et al*., in *Optical Interference Coatings*, OSA Technical Digest (Optical Society of America, Washington, DC, 2004), Paper TuF3.

9. J. B. Oliver, P. Kupinski, A. L. Rigatti, A. W. Schmid, J. C. Lambropoulos, S. Papernov, A. Kozlov, and R. D. Hand, in *Optical Interference Coatings*, OSA Technical Digest (Optical Society of America, Washington, DC, 2010), Paper WD6.

10. M. Henyk, D. Wolfframm, and J. Reif, Appl. Surf. Sci. **168**, 263 (2000).

11. M. Reichling, A. Bodemann, and N. Kaiser, Thin Solid Films **320**, 264 (1998).

12. R. Thielsch, A. Gatto, J. Herber, and N. Kaiser, Thin Solid Films **410**, 86 (2002).

13. G. G. Stoney, Proc. R. Soc. Lond. A **82**, 172 (1909).

14. J. W. Hutchison and T. Y. Wu, eds. *Advances in Applied Mechanics*, Vol. 29 (Academic Press, San Diego, CA, 1992).

15. M. Ohring, *Materials Science of Thin Films: Deposition and Structure*, 2nd ed. (Academic Press, San Diego, 2002), pp. 723–730.

16. S. Papernov and A. W. Schmid, J. Appl. Phys. **82**, 5422 (1997).

17. J. Proost and F. Spaepen, J. Appl. Phys. **91**, 204 (2002).

18. Y. Shen *et al*., Rare Met. Mater. Eng. **36**, 412 (2007).

19. J. B. Oliver and D. Talbot, Appl. Opt. **45**, 3097 (2006).

20. D. J. Smith, A. Staley, R. Eriksson, and G. Algar, in *Proceedings of the 41st Annual Technical Conference of the Society of Vacuum Coaters* (Society of Vacuum Coaters, Albuquerque, NM, 1998), pp. 193–196.

21. A. V. Tikhonravov and M. K. Trubetskov, OptiLayer Thin Film Software, Optilayer Ltd., http://www.optilayer.com (9 June 2005).